This article was downloaded by:
On: *22 January 2011*
Access details: *Access Details: Free Access*
Publisher *Taylor & Francis*
Informa Ltd Registered in England and Wales Registered Number: 1072954 Registered office: Mortimer House, 37-41 Mortimer Street, London W1T 3JH, UK

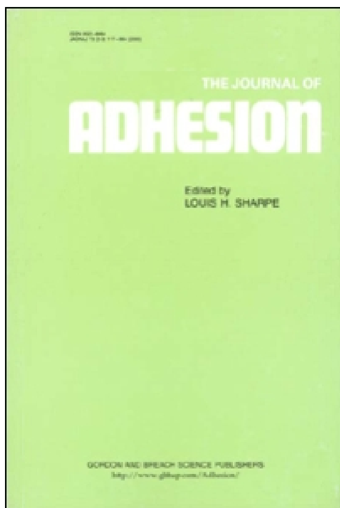

The Journal of Adhesion
Publication details, including instructions for authors and subscription information:
http://www.informaworld.com/smpp/title~content=t713453635

Dis-Bond Detection and the Possibility of Interfacial Stiffness Measurement with Real-Time Impulsive Stimulated Thermal Scattering

John A. Rogers[a]; Keith A. Nelson[a]
[a] Department of Chemistry, Massachusetts Institute of Technology, Cambridge, MA, USA

To cite this Article Rogers, John A. and Nelson, Keith A.(1995) 'Dis-Bond Detection and the Possibility of Interfacial Stiffness Measurement with Real-Time Impulsive Stimulated Thermal Scattering', The Journal of Adhesion, 50: 1, 1 — 24
To link to this Article: DOI: 10.1080/00218469508027110
URL: http://dx.doi.org/10.1080/00218469508027110

PLEASE SCROLL DOWN FOR ARTICLE

Full terms and conditions of use: http://www.informaworld.com/terms-and-conditions-of-access.pdf

This article may be used for research, teaching and private study purposes. Any substantial or systematic reproduction, re-distribution, re-selling, loan or sub-licensing, systematic supply or distribution in any form to anyone is expressly forbidden.

The publisher does not give any warranty express or implied or make any representation that the contents will be complete or accurate or up to date. The accuracy of any instructions, formulae and drug doses should be independently verified with primary sources. The publisher shall not be liable for any loss, actions, claims, proceedings, demand or costs or damages whatsoever or howsoever caused arising directly or indirectly in connection with or arising out of the use of this material.

J. Adhesion, 1995, Vol. 50, pp. 1–24
Reprints available directly from the publisher
Photocopying permitted by license only

© 1995 OPA (Overseas Publishers Association)
Amsterdam B.V. Published under license by
Gordon and Breach Science Publishers SA
Printed in Malaysia

Dis-Bond Detection and the Possibility of Interfacial Stiffness Measurement with Real-Time Impulsive Stimulated Thermal Scattering*

JOHN A. ROGERS and KEITH A. NELSON**

Department of Chemistry, Massachusetts Institute of Technology, Cambridge, MA 02139, USA

(Received February 14, 1994; in final form May 14, 1994)

Downloaded At: 12:39 22 January 2011

We describe a new, real-time, noninvasive method for dis-bond (delamination) detection which is based on a technique known as impulsive stimulated thermal scattering (ISTS). We first explain the ISTS technique and compare data from polyimide films tightly bound to silicon substrates with data from unsupported polyimide films. The observed differences in the data from these two cases are readily understandable and offer an unmistakable signature for delaminations. We demonstrate ISTS dis-bond detection by locating and mapping out randomly-distributed and spatially-fine regions of delamination in a polyimide film–silicon substrate system. Finally, we present two simple physical models of the interfacial region which comprehensively describe acoustic data from the tightly-bound and the unsupported samples. With insight from simulations using these models, we suggest how ISTS might be used to determine interfacial adhesion quality and we show how ISTS sensitivity to interfacial effects can be adjusted.

KEY WORDS: dis-bond; photo-acoustics; ultrasonic; interfacial stiffness; noncontact nondestructive evaluation; surface acoustic waves; adhesion; interphase.

INTRODUCTION

Reliable testing of adhesively bonded thin film microstructures is of vital importance for a fundamental understanding of complex interface chemistry and for practical applications in microelectronics and other industries. While there are many destructive tests of thin film adhesion,[1–5] there are relatively few noninvasive methods. Some of these nondestructive methods use thermal wave imaging,[6–10] but most are based on the generation and detection of ultrasonic disturbances using transducers or lasers (For reviews and descriptions of current state of the art in nondestructive testing, see Refs. 10–13.). When transducers are used, coupling fluids are usually needed to decrease the impedance mismatch between the transducer and the test part. The use of

*Presented at the Seventeenth Annual Meeting of The Adhesion Society, Inc, in Orlando, Florida, U.S.A., February 21–23, 1994.

**Corresponding author.

such fluids does not pose serious problems provided, of course, that they do not damage or alter the part being tested. For applications in areas such as microelectronics where sample contamination is of utmost concern and where film thicknesses are often on the order of hundreds of angstroms, it is difficult to imagine the use of coupling agents ever being acceptable. We believe the future of ultrasonic bond testing in thin films will be with laser-based methods, since the need for coupling fluids and mechanical contact with the sample are eliminated. In the most widely used laser-based testing method, [14–20] a short pulse is absorbed strongly at a sample surface to launch an acoustic wavepacket which propagates into the film and is reflected back and forth at opposite interfaces. Acoustic propagation is monitored through measurement of time-dependent changes in the reflectivity or position of one of the surfaces. The interfacial reflectivity measured from such experiments is related to the mechanical integrity of the bond. While this method is simple and straightforward, it imposes rather demanding requirements on the sample and the experimental apparatus when thin films are examined. For example, accurate characterization of a 1000-angstrom film requires an acoustic wavepacket width on the order of 100 angstroms. To excite and monitor such a disturbance effieciently, the film must absorb all of the excitation laser light in less than 100 A, and a laser pulse duration and detection time resolution of roughly 10 picoseconds is required. To meet these criteria, primarily metal films or samples with attached metal film transducers have been examined[14–20] with visible excitation and probe pulses derived from a picosecond or subpicosecond laser. The excitation-probe pulse sequence is repeated many times with variable probe delays, and the time-dependent sample response is recorded "point by point" on the time axis. Total data acquisition times of ten minutes or longer are typical.

Downloaded At: 12:39 22 January 2011

The ultrasonic method for thin film dis-bond location that we introduce here has many attractive features. First, the technique is entirely laser based and, therefore, does not require impedance matching agents or contact with the sample. Further, rather simple and inexpensive lasers can be used with conventional fast detection electronics to yield data collection with a single shot of the laser and millisecond acquisition times. Lateral spatial resolution as high as tens of microns along with the fast data collection rates makes it feasible to inspect completed multichip modules and microstructures directly. Finally, and perhaps most importantly, the sensitivity of this technique to delaminations actually increases as the film thickness decreases, making dis-bond detection in ultrathin (hundreds of angstroms) films possible.

The method is known as impulsive stimulated thermal scattering (ISTS)[21,22] and it has been used extensively in the past to study glass-forming bulk liquids.[23–26] In ISTS, two laser pulses are crossed at an excitation angle, θ, in an absorbing sample. The temporal and spatial overlap of the crossed pulses leads to a grating interference pattern with wavelength $\Lambda = \lambda_1/2\pi \sin(\theta/2) = 2\pi/q$ where λ_1 is the laser wavelength and q is the magnitude of the scattering wavevector. Absorption of the interfering excitation pulses leads to heat deposition that is impulsive on the time scale of excited material modes. Expansion that follows this mild heating drives acoustic and thermal responses with well defined wavevectors $\pm \mathbf{q}$. The temporal evolution of the material response is determined by time resolving the diffraction of a continuous wave probe. Figure 1 illustrates the experimental arrangement and Figure 2 shows typical data from a polymer thin film sample. The upper frame of Figure 2 shows acoustic

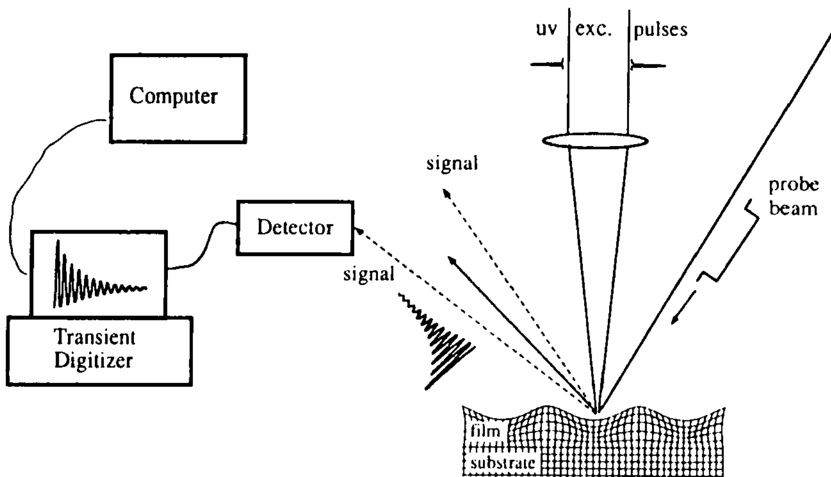

FIGURE 1 Experimental setup for real-time ISTS experiments on thin film coatings. Two excitation pulses are crossed and absorbed in the sample. The probe beam is spatially and temporally overlapped with the excitation pulses at the sample. The diffracted signal is time-resolved electronically with a fast photodiode and a transient digitizer.

Downloaded At: 12:39 22 January 2011

oscillations and decay. Since the acoustic wavelength is determined by the angle between the excitation beams, the measured frequency and damping rate can be used to calculate the complex phase velocity in a straightforward manner. As illustrated in Figure 2, even after the acoustic response is fully damped, the temperature modulation and an associated steady-state thermal expansion "grating" remain. Diffracted signal persists until thermal diffusion returns the system to equilibrium. The lower frame of Figure 2 shows data illustrating this thermal diffusion which typically occurs on microsecond time scales. The thermal diffusivity can be determined directly from this decay.

In this paper, we focus on the information available from the acoustic part of the ISTS data. In films whose thickness is comparable with the grating wavelength, acoustic motions excited by ISTS exhibit strong waveguide effects. This means that the overall response of the film is due to displacements associated with a number of acoustic waveguide modes (or normal modes), each with a distinct spatial character and propagation speed. (The character of a number of these modes is illustrated in Figures 4 and 6–7.) It can be shown that the acoustic phase velocity of each of these modes changes as the film thickness or the acoustic wavelength is varied. The particular way in which the phase velocities vary (that is, the dispersion in the phase velocity) is completely determined by the mechanical properties of the film, the mechanical properties of the substrate and by the properties of the film-substrate interface. As a result, measured dispersion can be inverted to determine these properties. For example, in previous work,[27] acoustic waveguide modes of polyimide films (DuPont's PI2555 or BTDA/ODA/MPD) tightly bound to silicon substrates were studied. ISTS was used to evaluate acoustic waveguide mode velocities as a function of acoustic wavevector and

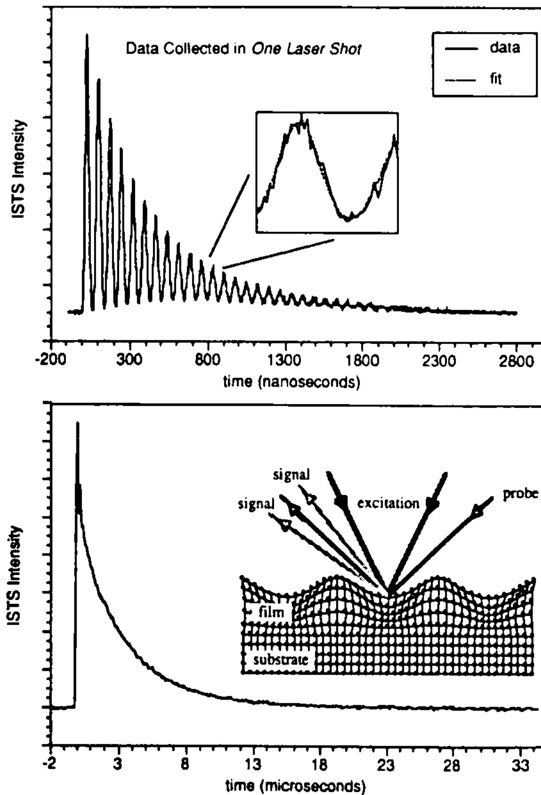

FIGURE 2 The upper frame shows ISTS acoustic data collected in one laser shot from a 1.56 micron unsuppported PI2555 film. The dashed line corresponds to a fit from which the acoustic frequency and damping rate are determined. The lower frame shows thermal diffusion data collected on microsecond time scales. The decay rate is a function of the thermal diffusivity of the film. The inset schematically illustrates the experiment.

Downloaded At: 12:39 22 January 2011

film thickness. Through a non-linear least squares fit of the measured dispersion to calculated dispersion, the intrinsic moduli of the films were determined. In another study, acoustic waveguide modes in unsupported films of PI2555 were investigated.[28,29] Again, ISTS was used to determine waveguide phase velocities as a function of film thickness and acoustic wavevector and the data were fit to calculate waveguide mode dispersion curves in order to determine the mechanical properties of the films. See Figure 3.

Although the elastic moduli (*i.e.*, the intrinsic mechanical properties) of the tightly bound and unsupported films determined in these two studies were found to be identical within experimental uncertainties, there are striking differences in the acoustic waveguide mode dispersion curve shapes which can be completely accounted for by the existence of tight mechanical coupling of the film to the substrate in the tightly-bound case and by the absence of any such coupling in the unsupported case. The differences in dispersion lead to dramatic differences in ISTS signals from

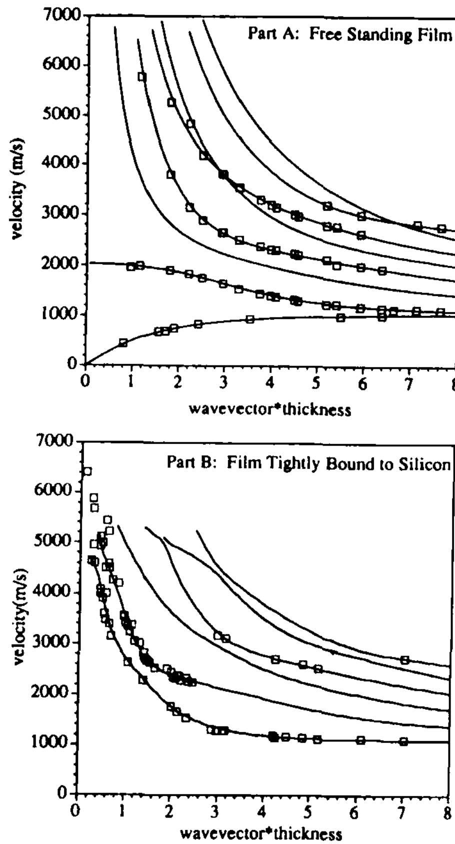

FIGURE 3 Data (symbols) and best fit acoustic velocity dispersion curves for unsupported (part A) and silicon-tightly bound (part B) PI2555 films. The striking differences between the acoustic properties in these two cases are due solely to the mechanical contact of the film to the substrate. The different dispersion characteristics provide a basis for delamination detection through ISTS.

Downloaded At: 12:39 22 January 2011

unsupported and tightly-bound films, and provides the basis for detection of delaminated regions in a film-substrate assembly. In this paper, we show how ISTS data can be used to detect delaminations and how changes in the experimental geometry allow film properties to be separated from interfacial properties. We demonstrate these capabilities by spatially resolving delaminations and mechanical inhomogeneities in a two-micron-thick polyimide film coated onto a silicon wafer. The results show that the ISTS method can be used to efficiently locate and map out delaminated regions which are indistinguishable by visual inspection from tightly-bound regions. In addition to this, two simple models for the interface are adopted that can describe cases of imperfect adhesion. One uses distributed springs and the other explicitly includes an additional material layer to model the interfacial region. The results suggest how it should be possible to use ISTS to determine interfacial stiffnesses in imperfectly bonded thin films.

EXPERIMENTAL RESULTS AND QUALITATIVE DESCRIPTION

Comparison of Experimental Results from Unsupported Polyimide Films and from Polyimide Films Tightly Bound to Silicon Substrates

As mentioned in the introduction, in previous work ISTS was used to examine acoustic waveguide modes in unsupported films[28,29] and films tightly bound to substrates.[27] In both cases, a theoretical model of the acoustic motions was described and used to determine intrinsic properties of the films. Specifically, ISTS was used to determine the phase velocity dispersion of the acoustic waveguide modes. Calculated phase velocity dispersion was fit to measured dispersion using a non-linear least squares fitting algorithm (Levenberg-Marquardt) with the values of the film elastic moduli (Young's modulus and Poisson's ratio) as the only adjustable parameters. Figure 3B summarizes results of a study of a tightly bound film-sub-strate system.[27] Figure 3A shows similar results for an unsupported film.[28,29] In both cases, very good agreement between calculated and measured dispersion was achieved, and the film moduli were evaluated to a high degree of accuracy. We also note that Figure 3 illustrates a very important feature of acoustic waveguides such as these. That is, for a given set of material properties, the number, phase velocity, and spatial nature of the acoustic waveguide modes all scale with an "effective" or dimensionless thickness defined by the product of the acoustic wavevector magnitude, q, and the film thickness, d. Because of this, the phase velocity dispersion can be experimentally evaluated either by collecting ISTS data at a single excitation angle (acoustic wavevector) in a number of films with different thicknesses, or by collecting data at a number of ISTS excitation angles in a single film. For example, the symbols in Figure 3 represent acoustic velocities determined from ISTS data such as those shown in the upper frame of Figure 2 with a wide range of wavevectors and thicknesses. This concept of effective film thickness is used below to motivate a qualitative understanding of the differences in dispersion curve shapes in the tightly-bound and unsupported cases.

Downloaded At: 12:39 22 January 2011

As previously mentioned, the elastic moduli of the tightly-bound and unsupported films determined from the fits shown in Figure 3 are identical within the several-percent experimental uncertainties. The striking quantitative and qualitative differences in the dispersion curves of Figure 3 are, therefore, due solely to mechanical boundary conditions and are not the result of different intrinsic film properties. Although all of the modes show different dispersion characteristics, we focus on qualitative explanation of differences in the slowest two modes since these dominate the ISTS data.[27-29] From Figure 3A, we see that the velocity of the lowest mode in the unsupported case decreases to zero as the acoustic wavevector-film thickness product (qd) approaches zero. As can be seen from Figure 4A, this mode (#0) involves primarily a transverse rippling of the film. As the effective thickness qd (*i.e.*, the thickness relative to the acoustic wavelength) decreases, the resistance of the film to this sort of motion decreases and, as a result, the velocity of the mode approaches zero for an infinitesimally thin film. On the other hand, from Figure 3B we see that in the tightly-bound case, the velocity of the lowest mode increases sharply and approaches the Rayleigh (surface) acoustic wave velocity of the substrate as qd approaches zero. In this case, as the effective film thickness decreases, the substrate becomes more involved in the motion

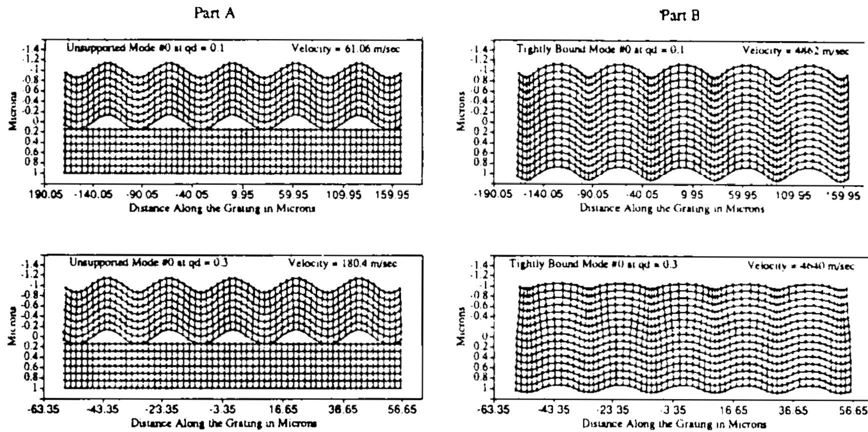

FIGURE 4 Lattice distortion diagrams for displacements associated with the lowest order waveguide mode for the unsupported (part A) and the silicon-tightly bound (part B) polyimide films at wavevector (q) times film thickness (d) values of 0.1 (upper frames) and 0.3 (lower frames). The striking differences in the spatial nature and phase velocities of the modes illustrated in parts A and B account for the sensitivity of the ISTS technique to interfacial properties in the small qd range. This allows for film-substrate delamination detection with ISTS. (In this figure and in similar ones to follow, a film thickness of one micron is assumed and displacements are displayed one micron into the substrate.)

Downloaded At: 12:39 22 January 2011

associated with the mode, resulting in an effective stiffening of the mode. See Figure 4B. Because of this, at very small values of qd the mode acquires properties of the silicon substrate, and takes on the substrate Rayleigh wave velocity at $qd = 0$. As a result, there is more than an order of magnitude difference between the velocities of the tightly-bound and unsupported films in the $qd \sim 1$ region. In fact, for the smallest qd value studied experimentally ($qd = 0.13$), these velocities differ by more than a factor of 60. To emphasize this, we display in Figure 5 ISTS data at a small qd value from tightly-bound and unsupported regions of a single sample. These data show the lowest order waveguide mode in the tightly-bound and unsupported cases which, at this particular qd value, have frequencies that differ by more than a factor of ten. Again, the tightly-bound film data show a higher frequency only because of the mechanical stiffening effect of the silicon substrate. Clearly, this provides an unmistakable ISTS signature for delaminations.

The second lowest mode in the unsupported case shown in Figure 3A rises and then levels off at a velocity slightly smaller than the film longitudinal velocity as qd decreases to values less than ~ 1. From Figure 6 we see that this mode (#1) is primarily longitudinal for small values of qd. However, because there is some transverse character due to the stress-free boundary conditions at the surfaces of the film, the mode velocity is always less than the intrinsic longitudinal velocity. In the tightly-bound case, the velocity of the second mode steadily increases with decreasing qd until, for the semi-infinite substrate case, this propagating mode is "cut off" at the transverse velocity of the substrate. The velocity of this mode increases because, as for the lowest mode, the substrate begins to influence the motion as the effective thickness of the film decreases. See Figure 6. The mode cut off occurs when mode energy is able to leak into the

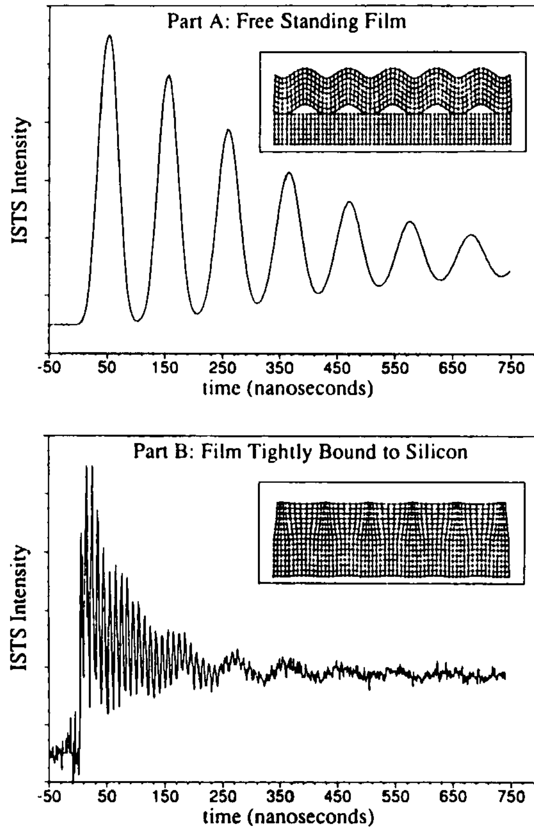

FIGURE 5 ISTS acoustic data collected in tightly bound and unsupported regions of a 2.16 micron PI2556 sample at a *qd* value of 0.61. The region of the film that is tightly bound to silicon (lower frame) has a frequency response that is much higher than that of the unsupported film (upper frame). The differences can be accounted for solely in terms of the mechanical stiffening of the waveguide by the silicon substrate.

Downloaded At: 12:39 22 January 2011

semi-infinite substrate. This criterion is met when the mode velocity becomes greater than or equal to the transverse velocity of the substrate. For the case of a polyimide film on silicon, then, the velocities of the second lowest modes for small *qd* values differ by roughly a factor of 2.5.

In contrast to mode properties for small *qd* values, as the effective thicknesses of the film increases, the film begins to act like a semi-infinite medium and the substrate is no longer important. In this regime, the acoustic velocities in both the tightly-bound and the unsupported modes take on the Rayleigh wave velocity (mode #0 and #1 for the unsupported case and mode #0 in the tightly-bound case) or transverse acoustic velocity (modes #2 and higher for the unsupported case and modes #1 and higher for the tightly-bound case) of the film. See Figure 3. Figures 4, 6, and 7 illustrate the evolution of the modes as the effective thickness increases. In the last of these figures, the spatial characteristics of the lowest three

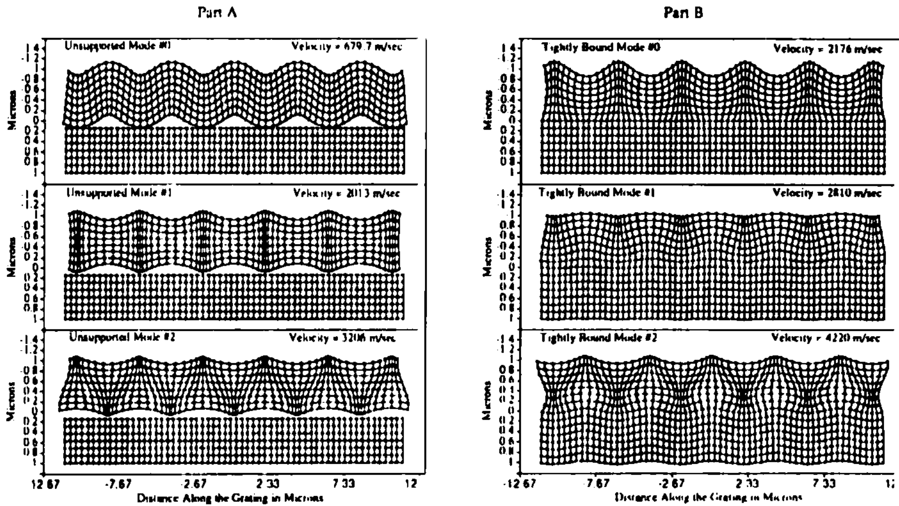

FIGURE 6 Lattice distortion diagrams for displacements associated with the lowest three waveguide modes in the unsupported (part A) and silicon-tightly bound (part B) polyimide films at a wavevector (q) times film thickness (d) value of 1.5. The differences in the spatial characters and the phase velocities of the unsupported and tightly bound modes at this qd combination are not as great as those observed at the smaller qd values given in Figure 4. Nevertheless, the differences exhibited even at this qd value allow unambiguous differentiation of the two cases with ISTS.

Downloaded At: 12:39 22 January 2011

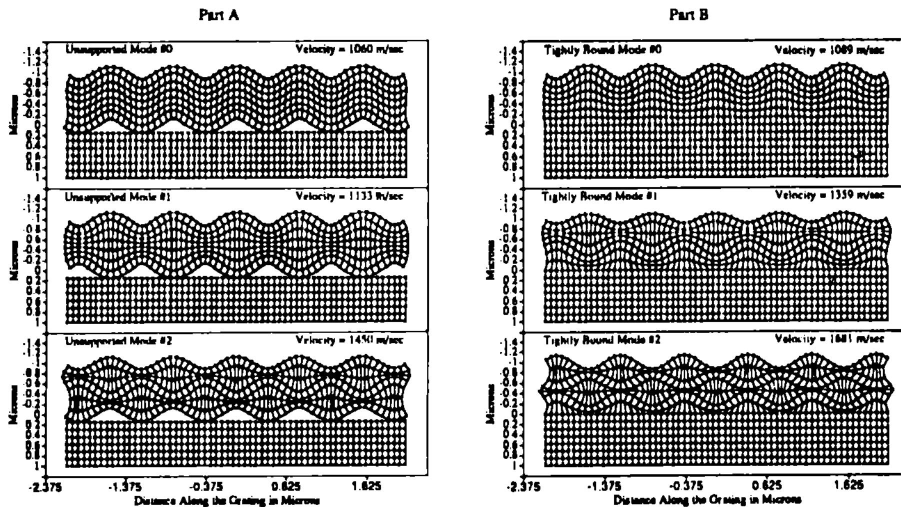

FIGURE 7 Lattice distortion diagrams for displacements associated with the lowest three waveguide modes in the unsupported (part A) and silicon-tightly bound (part B) polyimide films at a wavevector (q) times film thickness (d) value of 8.0. The similarity in the spatial characters and velocities of the modes in the two cases demonstrates the insensitivity of ISTS data to the interfacial region in this qd regime. ISTS measurements made in this regime provide intrinsic film properties, *i.e.*, elastic moduli, irrespective of interface quality.

modes at $qd = 8.0$ in the tightly-bound and unsupported cases are given. At this value of qd, motions of all of the modes vary rapidly along the direction normal to the surface of the film. Because of this, influence of the interface does not persist far into the film, and interfacial properties have little effect on the overall nature of the mode. The result is that at large acoustic wavevectors (large excitation angles in an ISTS experiment) or for very thick films, the measured mode phase velocities reflect intrinsic properties of the film. On the other hand, we showed that at small wavevectors (small excitation angles) or for very thin films, the mode velocities are sensitive functions of the substrate. This is very powerful because independent determination of film properties and delaminations can be achieved through a simple adjustment of the angle between the excitation beams, provided that a sufficiently wide range of qd values are experimentally accessible. This is determined by the wavelength of the excitation light and the film thickness. In practical terms, for ultraviolet excitation wavelengths, interfacial and intrinsic film properties can be separated in films with thicknesses between one and ten microns. For thinner films, interfacial properties and partial information about intrinsic mechanical properties can be extracted. For thicker films, intrinsic properties can be determined but it becomes difficult to reach effective thicknesses small enough to extract interfacial properties reliably.

Downloaded At: 12:39 22 January 2011

Demonstration of ISTS Delamination Inspection Capabilities

To demonstrate how ISTS delamination detection might work in practice, we fabricated a polyimide film–silicon substrate sample with unsupported and tightly-bound regions, as well as regions with a degraded interface. A polyimide-coated wafer was fabricated by spin coating and fully curing polyamic acid precursor solution on a silicon wafer. The wafer was then mounted in a Teflon jig apparatus and an acid etch mixture (6:1:1 mixture of $HF:HNO_3:CH_3OOH$) was used to remove silicon in selected locations, thereby creating regions of unsupported polyimide film.[28,29] Ordinarily, the etchant liquid is contained within a specified region of the wafer by a Teflon O-ring. By reducing the pressure with which the O-ring was pressed against the wafer, the acid etch was allowed to seep along the film-substrate interface at other locations to produce interfacially-degraded regions near the fully-etched regions. Thus, the treated wafer included some fully-etched regions, some regions which were not exposed to any etchant, and some interfacially-degraded regions. A picture of the resulting sample is shown in Figure 8. The ISTS method was used to scan this sample spatially both for delaminations and film mechanical inhomogeneities. We first collected data from the unsupported and tightly-bound regions, shown in Figures 9A and B, respectively. As expected with small ISTS excitation angles (*i.e.*, small effective thicknesses), the tightly-bound region shows a far higher acoustic frequency (in the lowest-order mode) than the unsupported region. ISTS data were then recorded at several spots in the interfacially-degraded region by simply translating the sample so that the laser beams probed different points on the wafer. The spatial resolution of the measurements was determined by the laser spot sizes which, for this set of experiments, were approximately 200 μm in diameter. Some of the results are shown in parts C, D, E and F of Figure 9. These data indicate that some spots in the region into which etchant liquid seeped are completely delaminated while others appear to be essentially tightly bound. These two

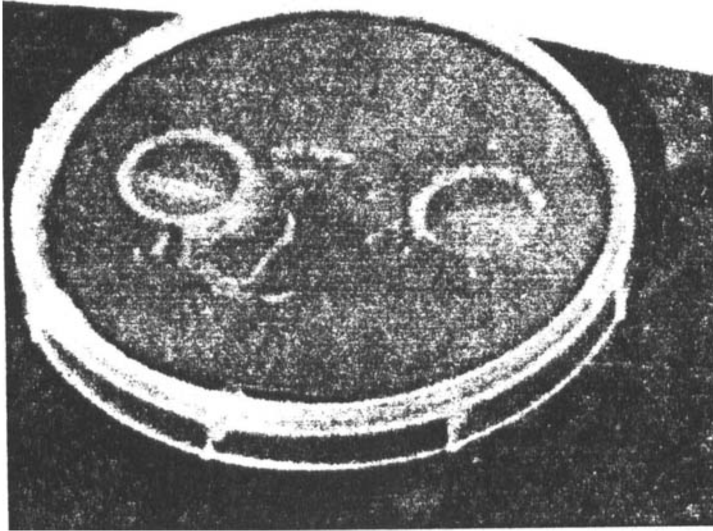

FIGURE 8 Photograph of polyimide-coated silicon wafer test sample. Two circular regions of the silicon were removed with an acid etch mixture. This etchant was allowed to creep along the film-substrate interface in other locations to produce irregularly-spaced regions of interfacial degradation. These regions were then mapped out using ISTS.

Downloaded At: 12:39 22 January 2011

kinds of spots appear different from the pristine sample, but cannot be distinguished from each other by eye. The results of this experiment indicate that at small angles ISTS can be readily used for delamination inspection purposes. They also suggest that the seepage of acid etch under the conditions described tends to create spots that are essentially tightly-bound or completely delaminated.

Since real-time ISTS has high spatial resolution and short data acquisition times it is possible to do much more than just perform "spot checks" for delaminations as described in the previous paragraph. By continuous translation of the sample, ISTS can be used to generate spatial images, or "maps" of film dis-bonding. We have generated such maps with ISTS, and a typical image is given in Figure 10. These data were acquired by monitoring ISTS response frequencies as a function of position by translating the sample with a calibrated two-way translation stage. Spatial locations at which large frequency shifts were observed (that is, of the magnitude illustrated in Figure 9) were determined from fast fourier transform analysis of the time domain data. The resulting data were used to generate the image shown in Figure 10. This image corresponds to an approximately 14 mm × 14 mm section of the wafer shown in Figure 8 and has a spatial resolution of approximately 40 microns. The curved boundary at the upper center of this figure represents the area of silicon substrate directly attacked and removed by the acid etch mixture (see Figure 8). The localized areas of film dis-bonding which appear near the edge of the etched area are due to seepage of the acid mixture along the film-substrate interface. As this image shows, disbonds only exist within approximately 2.5 mm of the region of the sample directly

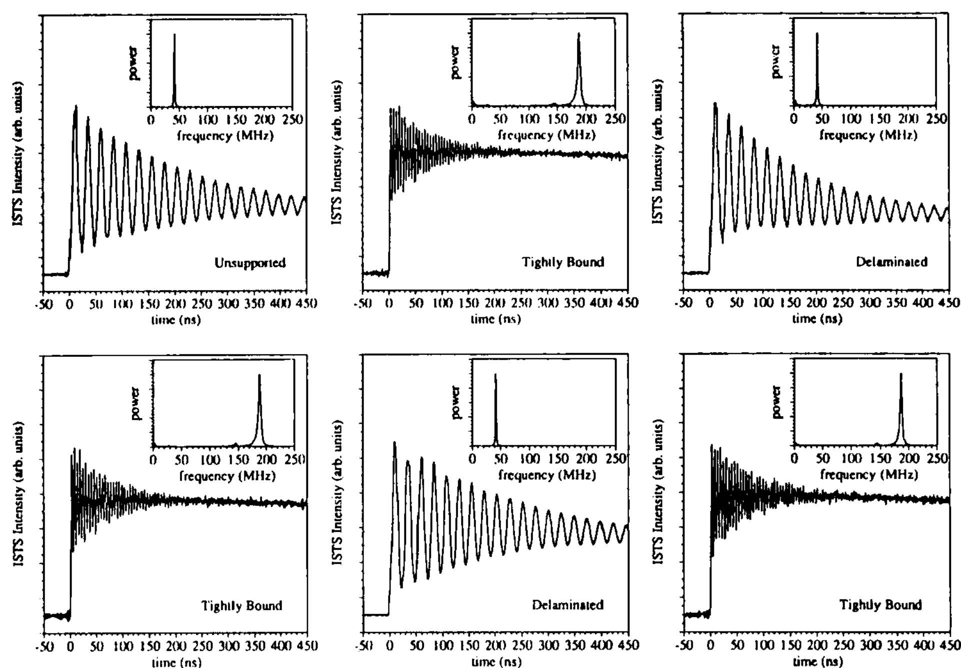

FIGURE 9 ISTS acoustic data collected at a small angle at several locations in the test sample shown in Figure 8. The first two frames give the response in the unsupported and tightly bound regions of the sample, respectively. The other scans show signal collected from different spots in the interfacially degraded region. The data allow delaminated spots and tightly bound spots which look identical by eye to be distinguished.

Downloaded At: 12:39 22 January 2011

exposed to the acid etch mixture. Outside of this area, the ISTS dis-bond map indicates only tightly-bound regions of film.

While the two examples described above focus on the interfacial sensitivity of ISTS measurements, by increasing the angle between the excitation beams, to increase the effective thickness of the film, we can eliminate the effects of the interface and of the substrate. In this case, spatial variation of ISTS response frequencies can be attributed solely to variation of intrinsic film material properties. In Figure 11 we show data recorded at large excitation angles at approximately the same spatial locations on the same sample inspected at small angles and described in Figure 9. The data in Figure 11 show that within $\sim 3\%$, the unsupported, fully-delaminated, and tightly-bound regions all have the same response. This result demonstrates that only the intrinsic properties of the film affect the response at large angles and that the film properties have not been significantly altered by the acid etch mixture. Data in Figures 9–11 provide a dramatic illustration of the ideas presented in the previous section. They show that a film can be spatially scanned at large excitation angles (large effective thicknesses) to locate film mechanical inhomogeneities and that data at small angles (small effective thicknesses) can be used to locate delaminations.

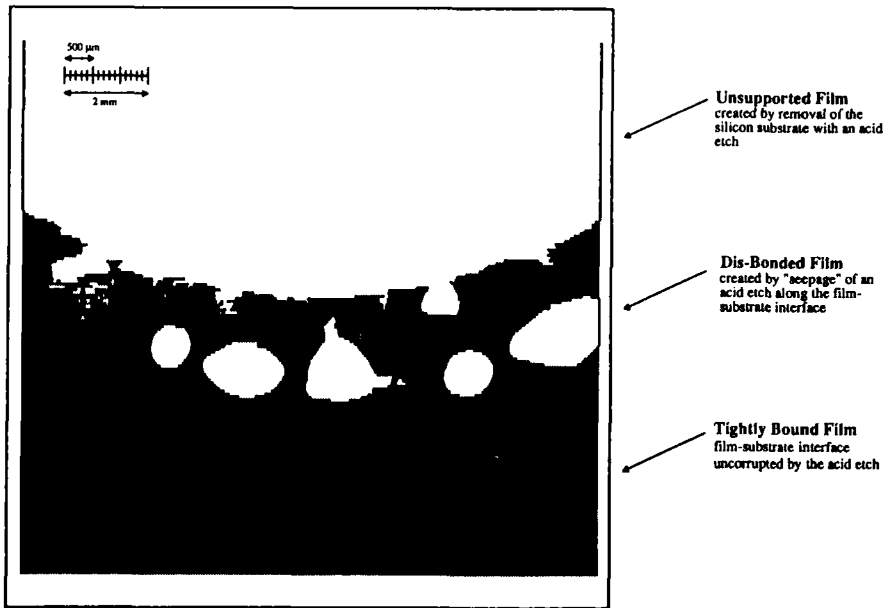

FIGURE 10 ISTS image, or "map" of dis-bonds in a polyimide film–silicon substrate system generated from ISTS data collected as the sample was spatially translated. Locations at which a large frequency shift (of the order shown in Figure 9) was observed were recorded and used to generate this image. The shaded regions correspond to tightly bound areas of film while the white regions correspond to locations of unsupported or disbonded film. The image represents an approximately 14 mm × 14 mm area of the sample near one of the two locations where the silicon substrate was removed using the acid etch mixture. (See Figure 8) The spatial resolution of this image is approximately 40 microns.

Downloaded At: 12:39 22 January 2011

THEORY

Adhesion Evaluation

The results thus far demonstrate that the two limiting cases of a tightly-bound film and a dis-bonded film can be distinguished readily through ISTS measurements with small scattering angles. More generally, intermediate cases with varying degrees of adhesion might be characterized. This would provide incisive fundamental insight into the connection between interface chemistry and interface mechanics, and could provide a nondestructive practical test through which interface degradation might be detected prior to complete delamination or device failure. In the next section, we use two simple models of the interfacial region to suggest that a procedure similar to the one used here might yield interfacial stiffnesses for films with intermediate adhesive quality.

There are many ways to describe and quantify the continuous transition from the delaminated film to the tightly-bound film. We will adopt two of these to investigate the ISTS response as a function of the integrity of the film-substrate bond. First, and most simply, we use a modification of an acoustic model used commonly to describe cracks, inclusions, and pores.[30] In this picture, the film and substrate are connected by massless

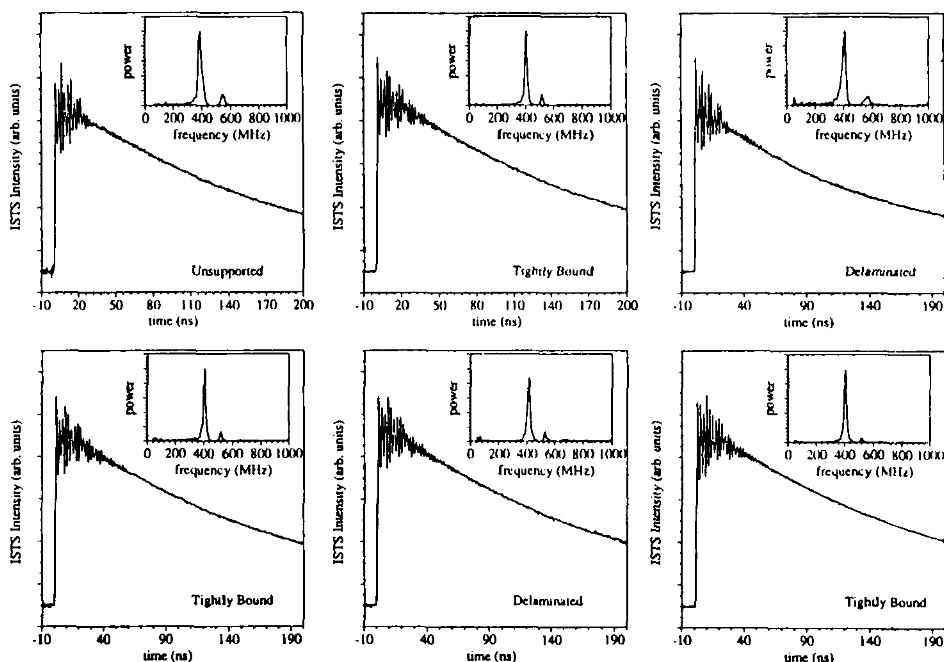

FIGURE 11 ISTS acoustic data collected with a large angle in several locations of the test sample shown in Figure 8. The first two frames give the response in the unsupported and tightly bound regions of the sample, respectively. The other scans show signal collected from approximately the same spots in the interfacially degraded region that are shown in Figure 8. These data illustrate that the nature of the interface does not affect the response of the film at large angles, and that the film properties are approximately homogeneous in this sample.

Downloaded At: 12:39 22 January 2011

springs whose spring constants characterize the interface. Although this model is perhaps the simplest possible description of the interface, there is no clear way to relate the magnitudes of the spring constants (*i.e.*, the linear mechanical response) to an intuitive sense for the strength (*i.e.*, the nonlinear response) of the interface. For this reason, we also present a model in which an "adhesive" material layer is added to describe the thin regions of film and substrate that are intimately involved in bonding.[31,32] The results of this model offer a more intuitive feel for the practical range of bond quality in which ISTS should be useful for adhesion evaluation.

Film-Substrate Bonding Modelled by Distributed Springs We first treat the film-substrate interface as a distributed massless spring which resists motion perpendicular and parallel to the film surface. See Figure 12. The degree to which interfacial motion is resisted is a function of two spring constants per unit area, κ_z and κ_y. This model is purely phenomenological and we do not suggest that it correctly describes the details of the interface. We do expect the qualitative trends exhibited by the model to be correct and because of this we limit our focus to these trends.

We assume that the ISTS excitation region is infinitely large, and we set the grating wavevector along the z axis and make the y axis perpendicular to the film surface. (See

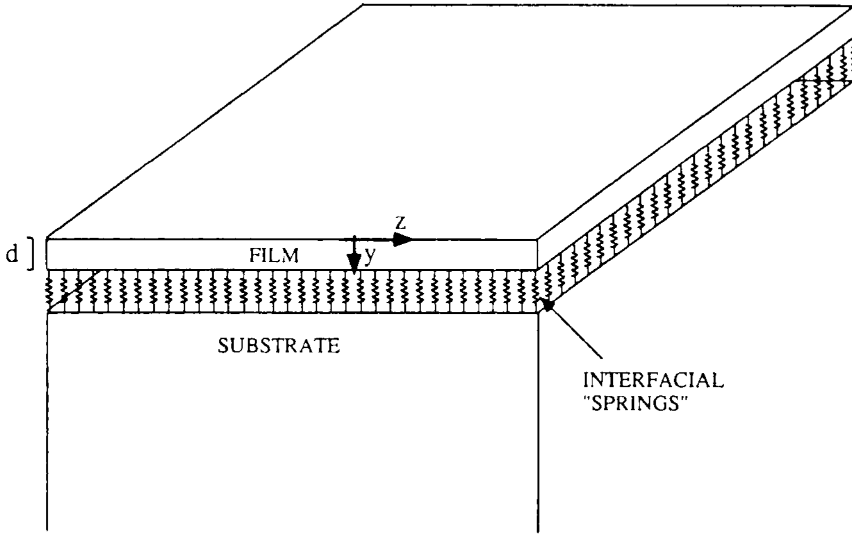

FIGURE 12 Diagram of the distributed spring model for interfacial adhesion. Infinitesimal massless springs at the interface are used to model adhesive properties. Spring constants per unit area $\boldsymbol{\kappa}_z$ and $\boldsymbol{\kappa}_y$ determine the coupling strength between film and substrate interfacial motions parallel and perpendicular to the bonding plane, respectively.

Downloaded At: 12:39 22 January 2011

Figure 12.) As a result, the material motions will be independent of x. Neglecting x components of tensors and vectors, the interfacial model prescribes the following boundary conditions at the interface (which lies at $y = d$) of the film-substrate system.

$$\sigma_{yy}(d^+) = \sigma_{yy}(d^-) \tag{1}$$

$$\sigma_{yz}(d^+) = \sigma_{yz}(d^-) \tag{2}$$

$$[u_z(d^+) - u_z(d^-)]\boldsymbol{\kappa}_z - \frac{1}{2}[\sigma_{yz}(d^+) + \sigma_{yz}(d^-)] = 0 \tag{3}$$

$$[u_y(d^+) - u_y(d^-)]\boldsymbol{\kappa}_y - \frac{1}{2}[\sigma_{yy}(d^+) + \sigma_{yy}(d^-)] = 0 \tag{4}$$

Here $\mathbf{u}$ is the displacement and $\boldsymbol{\sigma}$ is the stress. In the limit of infinitely stiff springs (*i.e.*, $\boldsymbol{\kappa}_z \to \infty$ and $\boldsymbol{\kappa}_y \to \infty$), these conditions reduce to stress and displacement continuity which describe the tightly-bound film.[27] When both spring constants are zero, the conditions reduce to the zero stress requirements used to describe the unsupported film analyzed previously.[28,29] Cases corresponding to imperfect adhesion are described by intermediate values of the stiffness constants. For example, a classical boundary condition for an interface which might be described as poorly adhering is defined as one with a slip interface.[33] That is, the interface of such a film resists motion perpendicular to the interface ($\boldsymbol{\kappa}_y$ large) but offers no resistance to motion along it ($\boldsymbol{\kappa}_z$ small).

The velocity dispersion and mode character are sensitive to the mechanical properties of the interface and in particular to the values of the distributed spring constants.

To demonstrate the changes that accompany variations in adhesion quality, we study the same polyimide-silicon system which was examined experimentally. (That is, the elastic moduli and densities are those of silicon and PI2555.) Calculations were carried out using the boundary conditions given in equations (1)–(4) for a variety of spring constant values using the computational techniques described in previous work.[27–29] In Figure 13 we display dispersion curves calculated for several values of $\kappa \equiv \kappa_y = \kappa_z$ to model what might be expected for imperfect adhesion. Note that phase velocity changes are most pronounced for the lowest two acoustic modes, and especially for the lowest mode. This is advantageous since these are precisely the modes that are efficiently excited and probed in a thin film ISTS experiment using excitation light that is strongly absorbed by the film and probe light that is not. Also note that the phase velocities of these lowest two modes are weak functions of κ for large qd values (> 3.0) and are strong functions of κ for small qd values (< 1.5).

Examination of the spatial character of the modes yields a more thorough understanding of the problem. By displaying the displacements of the lowest mode as the adhesion quality changes, we illustrate the changes induced by interfacial effects. Grid distortion diagrams of the lowest mode displacements at $qd = 0.5$ for three intermediate adhesion cases are displayed in Figure 14. We see that adhesion acts to couple displacements in the film to those in the substrate. As the spring constant is increased, the magnitude of the interfacial motion decreases until it approaches the very small value characteristic of the tightly-bound case. (The tightly-bound and the unadhered cases at $qd = 0.5$ are given in Figure 15). Naturally, the phase velocities increase as this coupling increases since the silicon is much stiffer than the polyimide.

Downloaded At: 12:39 22 January 2011

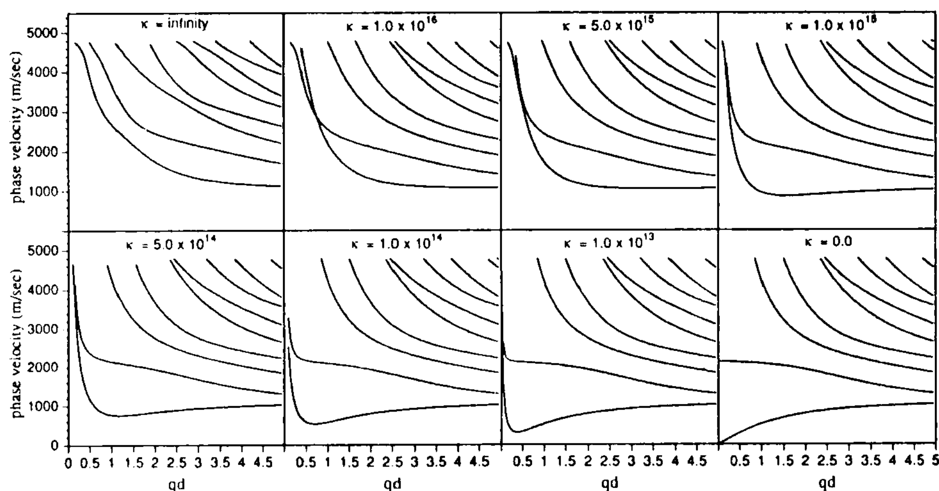

FIGURE 13 Dispersion curves for the polyimide film–silicon substrate system with the interfacial boundary modelled by distributed springs with stiffnesses per unit area $\kappa = \kappa_y = \kappa_z$. Each plot corresponds to a different value of κ. The upper left frame corresponds to the tightly bound case, and the lower right corresponds to the delaminated case. The other frames correspond to intermediate cases, with the adhesion quality decreasing on the top and bottom rows from left to right. The value of κ in MKS units is given in each frame.

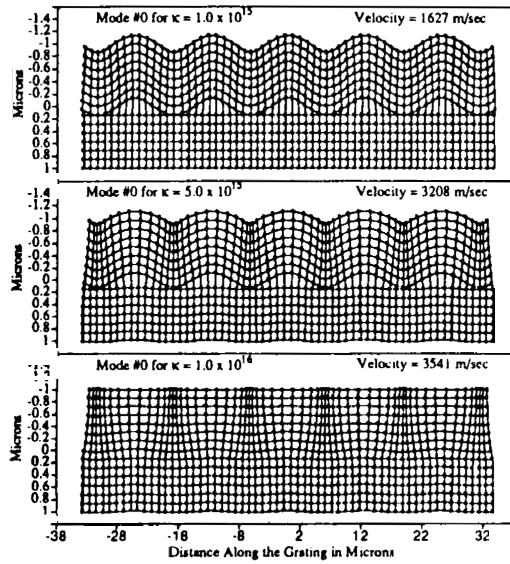

FIGURE 14 Lattice distortion diagrams of the lowest-order mode at $qd = 0.5$ for three different $K \equiv K_y = K_z$. As K increases, coupling to the substrate becomes stronger and, as a result, the velocity increases. The value of K in MKS units is given in each diagram.

Downloaded At: 12:39 22 January 2011

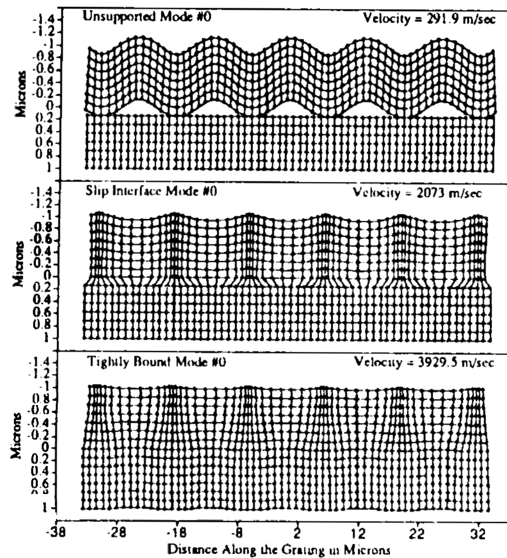

FIGURE 15 Lattice distortion diagrams of the lowest-order mode at $qd = 0.5$ for the delaminated, slip interface, and tightly bound cases. At this value of qd, the degree of the film-substrate bonding has significant effects on the spatial nature and velocity of the mode.

The disappearance of interfacial effects as qd gets large is illuminated with displacement diagrams for the lowest mode as a function of qd. We study the displacement fields of the lowest order mode for the delaminated, slip interface, and tightly bound films. Figure 15 gives grid distortion diagrams describing displacement fields for these three cases at $qd = 0.5$. For this value of qd, large phase velocity differences exist. For the delaminated case, the lowest mode consists of primarily transverse motions and is completely decoupled from the substrate. The slip interface film shows decoupling along the plane defined by the interface, but the σ_{yz} stress is non- zero at the interface, and the u_y displacement at the interface is continuous. This forces the mode to take on longitudinal character similar to the second lowest mode in the unsupported case (see Figure 6A). The tightly-bound film is strongly coupled to the substrate and because of this the spatial nature of the mode is dominated by the presence of the substrate. It is clear that in this small qd regime, the modes have distinctly different displacement fields and hence different velocities. To see what happens as qd is increased, we show distortion diagrams of the same lowest-order mode in each of the three samples at $qd = 1.0$, $qd = 2.0$, $qd = 4.0$, and $qd = 8.0$ in Figure 16. As qd gets larger, the slip interface and delaminated cases begin to exhibit close similarities. Although the delaminated case always has a displacement field quite different from the other two, for $qd = 8.0$ we see that motion near the surfaces of the delaminated film is similar to air side displacements in the other two cases. In fact, in this large qd regime, all of the modes begin to take on the film Rayleigh wave velocity and displacement field. In the case of the delaminated film, Rayleigh waves propagate on both free surfaces. Perturbations at the interface do not disrupt the Rayleigh wave on the air side of the film in the slip interface or the tightly-bound cases because this motion is well localized at the surface of the film. For this reason, all three cases yield waves with the same velocity and we see that the displcement field for the delaminated case is only superficially different from those for the slip interface and the tightly-bound cases. Since we adjust our position along qd by adjusting the excitation beam crossing angle, the acoustic response at high qd can be measured to evaluate film properties and the response at low qd can be used to determine interfacial information. This is, of course, completely consistent with experimental observations presented in Section II.

Downloaded At: 12:39 22 January 2011

Film-Substrate Bonding Modelled by an Interfacial Material layer Another simple way to describe adhesion is to introduce a distinct material layer at the interface.[31,32] In this model, the boundary conditions for stress and displacement between the interfacial layer and the film and substrate are characteristic of tightly-bound systems, and the strength of adhesion is related only to the mechanical stiffness of the layer. For example, when the interfacial layer has very low moduli, then the film is more weakly coupled to the substrate than when the interfacial modulus is high. In this sense, the interfacial layer description is very similar to the distributed spring model and, in fact, shows qualitative trends similar to those discussed in detail in the last section. The motivation for presenting the interfacial material layer model is to yield an intuitive feel for the physical nature of the interface when drastic changes in the shapes of the dispersion curves occur.

Modelling the acoustic properties of the layered waveguide is a straightforward but lengthy extension of the treatment given earlier.[27-29,31,32] We present the results in

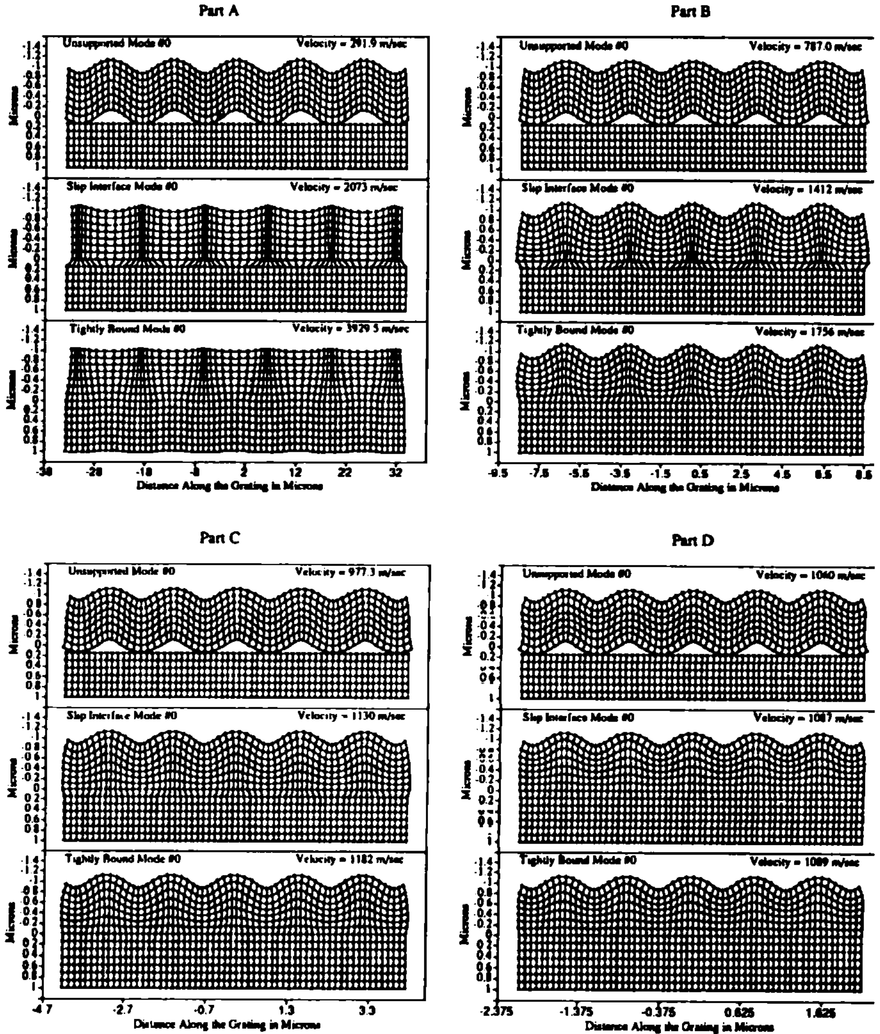

FIGURE 16 Lattice distortion diagrams of the lowest mode at $qd = 1.0$ (Part A), 2.0 (Part B), 4.0 (Part C), and 8.0 (Part D) for the delaminated, slip interface, and tightly bound cases. The trend is toward decreasing substrate influence as the value of qd increases. In particular, for $qd = 8.0$ when the effects of the substrate are minimal, all of the modes take on the same phase velocity, and the spatial characters of the modes closely resemble those of a Rayleigh wave (a surface wave characteristic of a semi-infinite substrate).

Figure 17. This figure illustrates the behavior of the three lowest acoustic modes that propagate in a one micron polyimide coating on a silicon wafer as the modulus and density of a 10 nm thick interfacial layer is changed. We have assigned seven different sets of mechanical properties, given in Table I to this interfacial layer. These range from the properties of silicon to the properties of a glass-forming liquid just below its glass transition temperature. Figure 17 shows the dispersion of the lowest three modes in

Downloaded At: 12:39 22 January 2011

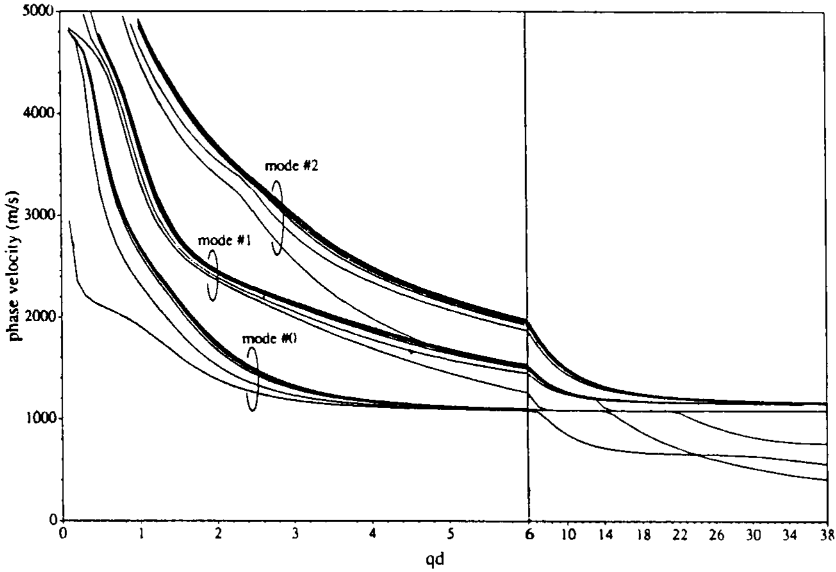

FIGURE 17 Dispersion curves for the lowest three modes propagating in a polyimide film–silicon substrate system with the interface modelled by a material layer 10 nm thick with a variable modulus. Each curve in a group corresponds to a different set of interfacial layer properties. These properties are listed in Table I. Since the dispersion is sensitive to the mechanical properties of the interfacial layer for a range of realistic parameters, ISTS should be able to characterize adhesion quality.

Downloaded At: 12:39 22 January 2011

each of these seven cases. Each curve in a set represents the results for a waveguide with given interfacial moduli. The curve with the highest phase velocity in each set corresponds to the case that the interfacial layer has the properties of silicon. The next lowest curve, which essentially overlaps with the highest curve, represents results when

TABLE I
Mechanical properties of the interfacial layer used in the simulations

Interfacial Material	Longitudinal Velocity (m/s)	Transverse Velocity (m/s)	Density (kg/m^3)
Silicon	8945	5341	2330
Quartz	6050	4100	2650
BTDA/ODA-MPD (PI2555)	2970	1150	1450
High Density Polyethylene	2430	950	957
Triphenylphosphite at 230 K	2000	700	1000
Triphenylphosphite at 245 K	1800	500	1000
Triphenylphosphite at 270 K	1600	200	1000

the interfacial layer has the properties of quartz. The interfacial properties for the next curve are those of the polyimide film, and the interfacial properties characterizing the next curve are those of high density polyethylene. The following two curves have interfacial properties between high density polyethylene and the interfacial layer of the lowest curve which has properties of the glass-forming liquid triphenylphosphite just below its glass transition temperature.[25]

Figure 17 shows several notable features. First, while changes in the dispersion of every mode are observable, the changes are most drastic for the lowest mode, which is consistent with results using the interfacial spring model of the previous section. Furthermore, in the large effective thickness (*qd*) limit, the phase velocities approach either the Rayleigh wave or transverse velocity of the film or slower velocities. These slow modes are not present in the interfacial spring model because they involve motion largely confined to the interfacial material layer. As such, they will not be excited efficiently with ISTS when the excitation pulses are absorbed in (and, therefore, most directly drive motions in) the film itself. As a result, the conclusion that interfacial effects disappear at large effective film thicknesses remains valid provided that, primarily, it is the film that is driven by the excitation pulses. Finally, the results in Figure 17 indicate that in order to induce changes in the shapes of the dispersion curve as drastic as those in the last few frames of Figure 13, the modulus of the interfacial layer must be quite low. (This can also be seen in the interfacial spring model by using an assumed spring length to calculate effective moduli of the distributed spring "layer".) In fact, velocity shifts of the magnitude seen for the four stiffest interfacial layers can be accounted for through adjustments of the film modulus. Therefore, provided that the film moduli are known, or provided that the adhesion is sufficiently weak (*i.e.*, characterized by interfaces with moduli in the range of the last three entries in Table I) ISTS will permit determination of the degree of adhesion of imperfectly bound films.

Finally, we note that the interfacial material layer model described in this section applies directly to systems where an adhesive or other adherent layer is used to promote bonding between film and substrate. In this case, ISTS can be used to monitor the hardening of the adhesion-promoting layer. To illustrate this, calculations described above were repeated for an interfacial layer 50 nm thick, which in this case represents the adhesive layer bonding the film to the substrate. The results are given in Figure 18. Phase velocity shifts due to changes in interfacial material modulus are easily quantifiable with ISTS.

Downloaded At: 12:39 22 January 2011

Film-Substrate Compatibility for ISTS Measurements

To this point, we have focussed on the polyimide-silicon system. To demonstrate that the conclusions are not dependent on a layered system with widely differing mechanical properties, we briefly discuss the case of a polyimide film–polyimide substrate system. For this illustration, we take the mechanical properties of the film to be *identical* to those of the substrate and, for convenience, use the interfacial material layer model for the interface. The calculated dispersion of the lowest order mode for this waveguide using the interfacial material properties given in the first five entries of Table I is given in Figure 19. When there is tight binding, the lowest order mode is dispersionless and takes on the Rayleigh wave velocity of the film. For cases of imperfect bonding, in the

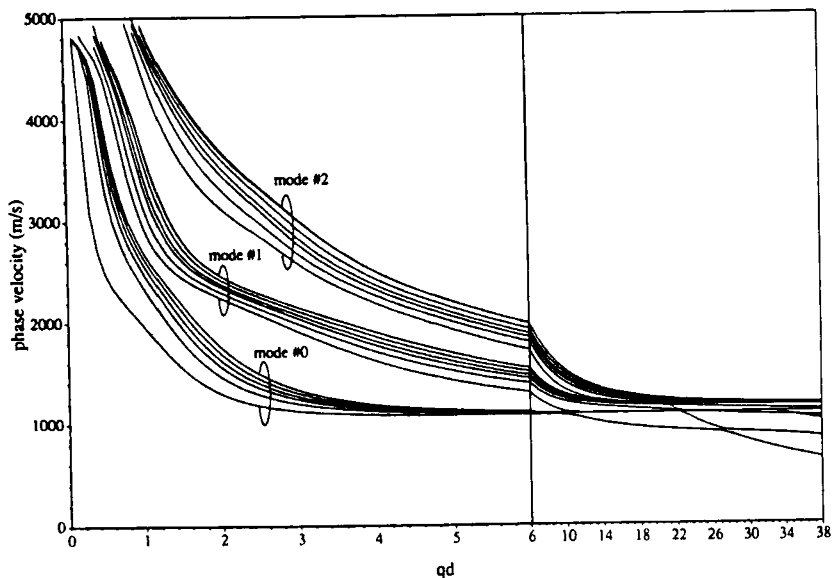

FIGURE 18 Dispersion curves for the lowest three modes propagating in a polyimide film–adhesion promoter–silicon substrate system. In this case, the adhesion-promoting layer is 50 nm thick. Each curve in a group corresponds to a different set of adhesion promoter layer properties. These properties are listed in Table I. Since the dispersion is sensitive to the mechanical properties of the adhesion promoter for a range of realistic parameters, ISTS should be able to characterize the mechanical integrity of this layer.

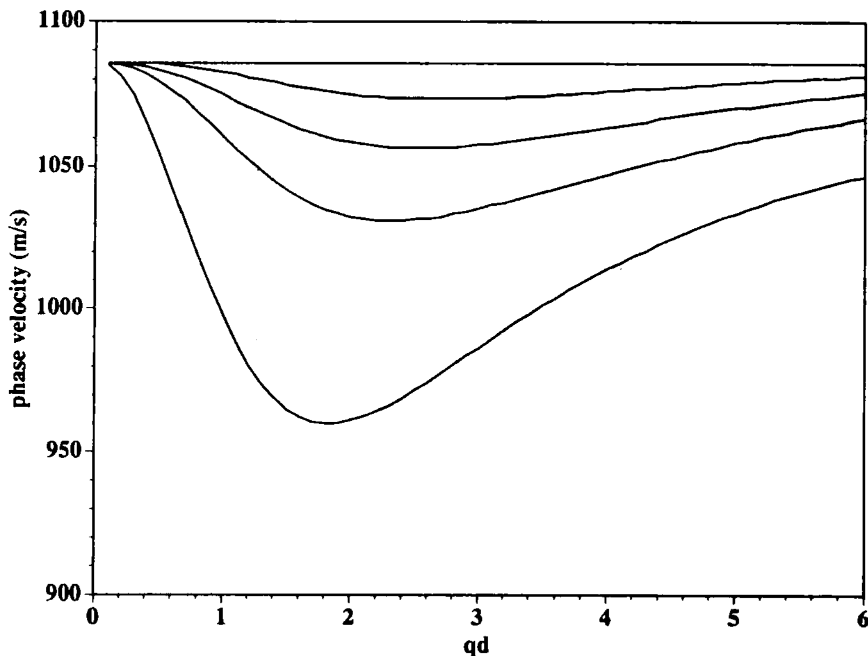

FIGURE 19 Calculated dispersion of the lowest-order acoustic mode for a polymer film–polymer substrate waveguide. The interface is modelled by an interfacial material layer. Each curve corresponds to a different set of mechanical properties for this interfacial layer. These results illustrate that an acoustic impedance mismatch between film and substrate is not necessary for interfacial bonding effects to alter significantly the mode phase velocities. It also demonstrates that conclusions based on the study of the polymer-silicon system are generally applicable to many other waveguides.

Downloaded At: 12:39 22 January 2011

small *qd* region there is a dip in the phase velocity. The position and depth of this dip are sensitive functions of the interfacial material properties. On the other hand, at large values of *qd* the velocities in each case approach the Rayleigh wave velocity of the film and are independent of interfacial properties. This simple example demonstrates that an acoustic mismatch is not necessary for ISTS interfacial measurements, and that conclusions arrived at through a study of the polyimide-silicon structure should apply to a wide range of other systems.

CONCLUSIONS

Through a comparison of data recorded from free-standing polyimide films with those taken from polyimide films tightly bound to silicon substrates, we have explained how the ISTS method can be used to detect delaminations. This capability was demonstrated through inspection of a polyimide-coated silicon wafer sample with irregularly-spaced delaminations. In addition to identifying delaminations, we have also suggested how similar data might be used to ascertain bonding quality in imperfectly-adhered films. In particular, we introduced two simple models to describe imperfect adhesion, and used them to predict the sensitivity of the ISTS experiment to interfacial stiffnesses. Experiments are underway to examine a series of films with different degrees of adhesion which will allow these ideas to be tested.

In addition to demonstrating interfacial effects on thin film ISTS data, we showed how to adjust the sensitivity of the ISTS experiment to these properties. This permits separate determination of film and adhesion properties. For example, by collecting ISTS data at one small and one large excitation angle, time-dependent changes in adhesion quality and in film properties could be separated and quantified as fabrication and cure procedures are under way. Alternatively, since the data acquisition rates are high and the spatial resolution is fine, pre-fabricated films could be spatially scanned at a large excitation angle for evaluation of film homogeneity. At small angles, a similar procedure could be used to probe the integrity of the film-substrate interface at various points across the sample. Both of these capabilities were demonstrated.

Downloaded At: 12:39 22 January 2011

Acknowledgements

This work was partially supported by NSF Grant No. DMR-9002279 and by the Donors of the Petroleum Research Fund, administered by the American Chemical Society. We also acknowledge support from the MIT Electronics Packaging Program. One of the authors (J. A. R.) has been supported by an NSF doctoral fellowship.

References

1. D. Suryanarayana and K. L. Mittal, *J. Appl. Polymer Sci.* **29**, 2039 (1984).
2. R. Narechania, J. Bruce and S. Fridmann, *J. Electrochem. Soc.* **132**, (1985).
3. L. B. Rothman, *J. Electrochem. Soc.* **127**, 2216 (1981).
4. M. G. Allen and S. D. Senturia, *J. Adhesion* **29**, 219 (1989).
5. M. G. Allen, Ph.D. Thesis, Massachusetts Institute of Technology, (1989).
6. A. C. Tam and H. Sontag, *Appl. Phys. Lett.* **49**, 1761 (1986).
7. D. L. Balageaus, J. C. Krapez and P. Cielo, *J. Appl. Phys.* **59**, 348 (1986).
8. J. P. Monchalin, J. L. Parpal, L. Bertrand and J. M. Gagne, *Appl. Phys. Lett.* **39**, 391(1981).
9. W. P. Leung and A. C. Tam, *J. Appl. Phys.* **63**, 4505 (1988).
10. C. C. H. Guyott, P. Cawley and R. D. Adams, *J. Adhesion* **20**, 129 (1986).

11. D. E. W. Stone. Technical Report 86058, Royal Aircraft Establishment, Ministry of Defence, Farnborough, Hants, UK (1986).
12. R. D. Adams and P. Cawley, in *Bonding and Repair of Composites*, J. Herriot, Ed. (Butterworth, London, 1989), p. 125.
13. Journal of Nondestructive Evaluation, Special Issue on Modeling and Ultrasonic Characterization of Interfaces, Guest Editor S. I. Rokhlin, Vol. 11, Nos. 3/4, Dec. 1992.
14. H. T. Grahn, H. J. Maris and J. Tauc, *IEEE J. Quant. Elec.* **25**, 2562 (1989).
15. C. Thomsen, H. T. Grahn, H. J. Maris and J. Tauc, *Phys. Rev. B* **34**, 4129 (1986).
16. G. L. Eesley, B. M. Clemens and C. A. Paddock, *Appl. Phys. Lett.* **50**, 717 (1987).
17. C.-D. Zhu, H. J. Maris and J. Tauc, in *Phonons 89*, S. Hunklinger, W. Ludwig and G. Weiss, Eds. (World Scientific, Singapore, 1990), p. 498.
18. O. B. Wright and K. Kawashima, *Phys. Rev. Lett.* **69**, 1668 (1992).
19. M. J. Banet, J. A. Rogers, C. Mindas and K. A. Nelson, unpublished.
20. M. J. Banet, Ph.D. Thesis, Massachusetts Institute of Technology, (1993).
21. H. J. Eichler, P. Gunter and D. W. Pohl, *Laser-Induced Dynamic Grating* (Springer, Berlin, 1986).
22. K. A. Nelson and M. D. Fayer, *J. Chem. Phys.* **72**, 5202 (1980); K. A. Nelson, D. R. Lutz, M. D. Fayer and L. Madison, *Phys. Rev. B* **24**, 3261 (1981).
23. I. C. Halalay and K. A. Nelson, *J. Chem. Phys.* **97**, 3557 (1992).
24. Y.-X. Yan, L.-T. Cheng and K. A. Nelson, *J. Chem. Phys.* **88**, 6477 (1988).
25. S. M. Silence, S. R. Goates and K. A. Nelson, *Chem. Phys.* **149**, 233 (1990).
26. A. R. Duggal and K. A. Nelson, *J. Chem. Phys.* **94**, 7677 (1991).
27. A. R. Duggal, J. A. Rogers and K. A. Nelson, *J. Appl. Phys.* **72**, 2823 (1992); A. R. Duggal, J. A. Rogers, K. A. Nelson and M. Rothschild, *Appl. Phys. Lett.* **60**, 692 (1992); J. A. Rogers, S. M. Thesis, Massachusetts Institute of Technology, (1992).
28. J. A. Rogers and K. A. Nelson, *J. Appl. Phys.* **75**, 1534 (1994).
29. J. A. Rogers and K. A. Nelson, *Appl. Phys. A.*, in press.
30. J.-M. Baik and R. B. Thompson, *J. Nondestr. Eval.* **4**, 177 (1984).
31. S. I. Rokhlin and Y. J. Wang, *J. Acoust. Soc. Am.* **89**, 503 (1991).
32. R. D. Weglein and A. K. Mal, *Proc. IEEE Ultrasonics Symp.*, 823 (1987).
33. G. J. Kuhn and A. Lutsch, *J. Acoust. Soc. Am.* **33**, 949 (1961).

Downloaded At: 12:39 22 January 2011